J Nanopart Res (2012) 14:933
DOI 10.1007/s11051-012-0933-2

RESEARCH PAPER

Physical and chemical properties of $Co_{n-m}Cu_m$ nanoclusters with $n = 2$–6 atoms via ab-initio calculations

Marcos Pérez · Francisco Muñoz · José Mejía-López · Gerardo Martínez

Received: 8 November 2011 / Accepted: 18 May 2012 / Published online: 10 June 2012

Abstract We present ab-initio density-functional calculations of the structural, magnetic, and chemical properties of cobalt–copper clusters (1 nm in size) with two to six atoms. We applied several search methods to find the most stable configurations for all stoichiometries. Particular attention is given to the relation between the geometric and magnetic structures. The clusters behavior is basically governed by the Co–Co interaction and to a lesser extent by the Co–Cu and Cu–Cu interactions. A tendency for Co-clumping is observed. Such information is quite relevant for segregation processes found in bulk Co–Cu alloys. For a given cluster size, magnetic moments increase mostly by $2\mu_B$ per Co-substitution coming from the cobalt *d*-states, while for some cases *s*-electrons give rise to *itinerant magnetism*. Magnetic moment results are also consistent with the ultimate jellium model because of a 2D to 3D geometrical transition. The chemical potential indicates less chemical stability with the Co atoms, while the molecular hardness can be linked mostly to the ionization potential for these small clusters.

Keywords Cobalt–copper ferromagnetic nanoclusters · Phase separation and segregation · Magnetic properties of nanostructures · Electronic structure of nanoscale materials · Modeling and simulation

M. Pérez · F. Muñoz · J. Mejía-López
Facultad de Física, Pontificia Universidad Católica de Chile, Av. Vicuña Mackenna 4860, Santiago, Chile
e-mail: jmejia@fis.puc.cl

M. Pérez · F. Muñoz · J. Mejía-López
Center for the Development of Nanoscience and Nanotechnology (CEDENNA), Av. Ecuador 3493, Santiago, Chile

G. Martínez (✉)
Instituto de Física, Universidade Federal do Rio Grande do Sul, Porto Alegre, RS CEP 91501-970, Brazil
e-mail: martinez@if.ufrgs.br

Introduction

The delicate balancing between the chemical composition and electronic degrees of freedom on metallic nanoclusters is a complex phenomenon. An accurate description of the structural configurations is demanded if one aims to extract optical, magnetic, or chemical properties from these novel materials. In particular, transition-metal nanoclusters have received special attention due to potential applications in high-density magnetic recording, nanocatalysis, and nanoelectronics (Ferrando et al. 2008). These clusters show a large variability involving structure and magnetism, because the magnetic properties are very sensitive to cluster sizes, bond angles, composition, and the interatomic separations, among others. Moreover, bimetallic clusters can have completely different properties if compared to their monoatomic counterparts. For example, Ghanty et al. (2010) proved that

for metallic Au, Cs, and Rb clusters, the diatomic clusters $Au_{19}Cs$ and $Au_{19}Rb$ are ionic semiconductors. Similarly, Mejía-López et al. (2009) showed that for Cu and Pt clusters which are nonmagnetic, the bimetallic $Pt_{12-n}Cu_n$ nanoclusters may be ferromagnetic depending on the Cu/Pt ratio.

The discovery of new phenomena, like giant magnetoresistance (Baibich et al. 1988) and the oscillatory exchange coupling in metallic multilayers (Parkin et al. 1990), on the other hand, have triggered a considerable amount of study on the physical properties of magnetic nanostructures. In the case of cobalt–copper particles at nanoscale sizes, for example, the presence of giant magnetoresistance (Berkowitz et al. 1992; Xiao et al. 1992) and ferromagnetism (Fan et al. 2004) was shown to depend on size, morphology and Co concentration, opening though many questions about the nature of these nanostructures (Miranda et al. 2003). Because of Co–Cu non-equilibrium properties, some of them evolve through spinodal decomposition (Miranda et al. 2006). In order to understand such complex behavior, it is desirable to see the influence of the relative concentration of Co and Cu atoms on the physical properties of such systems. Consequently, one of the main purposes of this study is to perform a systematic study of the interplay between structure, magnetic and chemical properties in small $Co_{n-m}Cu_m$ clusters having a size of $n \leq 6$ total atoms (with $0 \leq m \leq n$) using spin-polarized density-functional theory (DFT).

Experimental studies on Co–Cu nanosystems have been carried out for many different geometries: granular alloys (Rabedeau et al. 1993; Hickey et al. 1995), lamellar distributions (Miranda et al. 2003, 2006), multilayers (Ghosh et al. 2006; Bakonyi et al. 2009), Co nanoparticles within a Cu matrix (Cezar et al. 2003; Quaas et al. 2004) and Co adatoms on Cu surfaces (Zimmermann et al. 1999; Knorr et al. 2002; Rastei et al. 2007; Néel et al. 2008).

On the theoretical side, there exists only a few ab-initio studies about Co–Cu nanoclusters. For example, Wang et al. (2002) studied $Co_{18-m}Cu_m$ clusters ($0 \leq m \leq 18$) using a genetic algorithm and a Gupta-like many-body potential approach. They found that Cu atoms tend to occupy the surface, while Co atoms prefer the interior of the clusters. Ju et al. (2005), by using molecular dynamics (MD) simulations, studied the structural variation of large Co–Cu nanoparticles of two different Co concentrations (5 and 25 per cent). They found that the Co–Co bond length increases, the Co–Cu bond length decreases, and the Cu–Cu bond length does not change as the temperature is reduced. Lu et al. (2005) observed, using ab-initio calculations in $Co_{13-m}Cu_m$ clusters, that the magnetic moment is sometimes remarkably reduced due to antiferromagnetic (AF) couplings between the atoms.

Out of the mainstream ab-initio calculations, we found some earlier results for metallic clusters using the ultimate jellium model (Koskinen et al. 1995; Kolehmainen et al. 1997). Interestingly, when applied to our results on Co–Cu clusters, a close resemblance to the valence electrons behavior is observed due to a 2D to 3D geometrical transition, as explained in the text. This result is by no means trivial however, as the many-body jellium model is valid only in some special circumstances. In real metal clusters, the electron distribution is ultimately determined by the interplay between the electrons and the discrete ions.

Density-functional calculation approaches, on the other hand, have globally popularized the use of DFT methods in nanomaterials, particularly through generalized gradient approximations (GGA). The main reason is because when the electron density inhomogeneity $\rho(\mathbf{r})$ and its gradient contributions $\nabla\rho(\mathbf{r})$ are included, the exchange-correlation (XC) hole is better described, which entails considerable improvement over the local spin-density approximation (LSD). GGA stands for significant corrections of the energy results, giving better ground-state geometries, in particular when it describes bond breaking and bond formation in atoms and molecules. There exist several GGA implementations, such as PW86 (Perdew and Wang 1986), P86 (Perdew 1986), B88 (Becke 1988), PW91 (Perdew and Wang 1992) and PBE (Perdew et al. 1996a, b). Among these schemes, PBE has seemingly become a standard tool. Its improvements include an accurate description of the linear response of the uniform electron gas, a correct behavior under uniform scaling, and also a smoother XC potential. Such gradient-based density functionals have cured serious LSD flaws when it deals with total energy differences for some magnetic materials (Kübler 1981; Wang et al. 1985). For example, a straightforward LSD calculation will erroneously predict for metallic iron to be an fcc nonmagnetic ground-state instead of the bcc ferromagnetic ground-state, which is observed experimentally. GGA gives indeed the correct result in this case (Bagno et al. 1989).

In what follows, we use spin-polarized DFT calculations to study small Co–Cu bimetallic clusters with up to 6 atoms, and analyze their equilibrium configurations as a function of size and stoichiometry. The article is organized as follows: in "Computational details" section, we give the computational details outlining the search procedure of the most stable configurations and the physical descriptors used to analyze the data. In "Results and discussions" section, we present the results and discuss separately the sequence of clusters studied from dimers to hexamers. We also discuss in this section their binding energies and relative stabilities together with their magnetic and chemical properties. In "Conclusion" section, we give some conclusions and final remarks.

Computational details

The electronic structure calculations were performed in the framework of the DFT theory using the VASP algorithm: *Vienna Ab-initio Simulation Package* (Kresse and Hafner 1993; Kresse and Furthmüller 1996a, b) which implements a DFT code based on a pseudopotential plane-wave expansion. The projector augmented wave (PAW) method (Kresse and Hafner 1994; Kresse and Joubert 1999) and the PBE XC density functionals (Perdew et al. 1996a, b) for the spin-polarized GGA approximation were used. The 3*d* and 4*s* electrons of Co and Cu were treated as valence electrons. The energy cutoff was set at 270 eV, to obtain a reliable description of these systems. Grid calculations involved $100 \times 100 \times 100$ points. Simple cubic supercells with periodic boundary conditions and the cell size were chosen so that two neighboring clusters are separated by at least 14 Å vacuum space. This ensures that the interactions of a cluster and its periodic images are negligibly small. Unrestricted symmetry optimizations (in both geometry and spin numbers) were always performed using conjugate gradient and quasi-Newtonian methods, until all force components were less than 0.01 eV/Å. The electronic total energy convergence criterion was set to 10^{-6} eV, which is considered satisfactory for these kind of calculations.

To get the ground-state configuration and the lowest-energy isomers for each cluster size, at a given stoichiometry, we proceed in the following way: we first select several configurations, separated by the eigenvalues of the tensor of inertia, which is defined by

$$I_{ij} = \sum_{\ell=1}^{n} m_\ell \left[\mathbf{r}_\ell^2 \delta_{ij} - r_{i\ell} r_{j\ell} \right], \tag{1}$$

where $\{i, j\} = \{x, y, z\}$ are the cartesian coordinates, n is the total number of atoms in the cluster, $\mathbf{r}_\ell$ is the vector position (in Å) of the ℓ-esimal atom and m_ℓ are the corresponding atomic masses (in arbitrary units). The eigenvalues of Eq. (1) are always positive and can therefore be ordered from the lowest value: $I_{\min} \leq I_{\text{med}} \leq I_{\max}$. As we are interested only in the geometry of clusters, the m_ℓ values were chosen arbitrarily in order to differentiate two species of atoms in the bimetallic structure. By using $m_{\text{Co}} = 1$ and $m_{\text{Cu}} = 3$ we say that two structures, A and B, are configurationally separated when $|I_m^A - I_m^B| > 1$, for some $m \in \{\min, \text{med}, \max\}$.

Configurations separation using moments of inertia as a metric is widely used (Yang et al. 2006; Rogan et al. 2009). Though it does not constitute a true distance, each set of eigenvalues can be considered as a point in the configurational space with the rule stated above. This separation is a rather successful way to estimate distances between configurations, but it can fail in some pathological cases (like in the case of atoms lying along a line, for example).

Using this definition of distance, we first select randomly 100 non-equivalent geometric structures for each cluster size and stoichiometry. An additional empirical criterion was applied: the atomic distance between any two closest atoms had to be greater than 2 Å and less than 4 Å. This initial set of configurations was then force-filtered with a coarse energy precision (0.1 eV/Å) to obtain the 10 lowest-energy configurations, which were further refined thereafter by the higher precision force-filter (0.01 eV/Å).

The first descriptor we used is the binding energy E_{b}, which is defined as the energy per atom required to atomize the cluster into gas-phase atoms, that is

$$nE_b(n, m) = (n - m)E_{\text{Co}} + mE_{\text{Cu}} - E(n, m), \tag{2}$$

where n is the cluster size, m the number of Cu atoms, E_{Co}, E_{Cu}, and $E(n, m)$, are the total energies of an isolated Co atom, of an isolated Cu atom, and of a $\text{Co}_{n-m}\text{Cu}_m$ cluster, respectively. With this definition, at a given cluster size and for each stoichiometry, the structure with the *highest* binding energy is considered to be the ground-state.

The stability of clusters when the number of Cu atoms is changed, and for fixed cluster size, can be

studied through the relative stability parameter (Ganguly et al. 2008)

$$S(n,m) = E_b(n,m+1) - 2E_b(n,m) + E_b(n,m-1). \quad (3)$$

The local magnetic moments and the atomic electronic charge distributions were normally computed, unless it is otherwise mentioned, by integrating the related electronic densities in real space within a Wigner–Seitz radius of 1.3 Å, centered on each atom.

The chemical reactivity is usually characterized by two global descriptors (Parr and Pearson 1983; Parr and Yang 1984): one is the chemical potential, defined as $\mu_{chem} = (\partial E/\partial N)|_{V(\mathbf{r})}$, that gives information on the escaping tendency of electrons from the cluster, and which can be calculated in a discrete (symmetrized) form as

$$\mu_{\text{chem}} = \frac{E(N+1) - E(N-1)}{2}, \quad (4)$$

where N is the total number of electrons. The other is the molecular hardness, $\eta = \frac{1}{2}(\partial^2 E/\partial N^2)|_{V(\mathbf{r})}$, which measures the resistance of the cluster to changes on the electronic distribution. It can also be calculated in a discrete (symmetrized) form as

$$\eta = \frac{E(N+1) - 2E(N) + E(N-1)}{2}. \quad (5)$$

The inverse of the molecular hardness measures ease of charge transfer and it is associated with high polarizability. Moreover, η is related to the *chemical maximum hardness principle* (Chattaraj et al. 1995), which asserts that molecular systems usually tend to conform states of high hardness. See Kohn et al. (1996) for further remarks.

For comparison purposes we have also computed the ionization potential, $\text{IP} = E(N-1) - E(N)$, and the electron affinity, $\text{EA} = E(N) - E(N+1)$. We notice that $\mu_{\text{chem}} = -\frac{1}{2}(\text{IP} + \text{EA})$ and $\eta = \frac{1}{2}(\text{IP} - \text{EA})$.

Results and discussions

We have carried out extensive calculations for the ground-state and the first three low-energy isomers, i.e., different stable (*true minima*) configurations with the same stoichiometry. This is required for the comparison with experimental results. Isomers with different geometries and different magnetic moments, but close in energy, are likely to be present in the experiments in a mixed way.

In Table 1 we summarize, from dimers to hexamers, symmetry groups, binding energies, dissociation energies, magnetic moments, average bond lengths, ionization potentials, and electron affinities for the *ground-state* configurations of all the forthcoming depicted geometric structures.

Geometric structures

Dimers

The smallest clusters are the dimers. Despite the fact that this case has already been calculated, see previous reports (Castro et al. 1997; Fan et al. 1997; Wang et al. 2005; Datta et al. 2007), we describe it here to set up a principal result concerning structure and bonding. The redistribution of charge density strongly affects the general behavior of Co–Cu clusters. We also use this case to verify the quality and accuracy of our results by comparison with previous DFT results, as well as to experimental available data. In Fig. 1 we plot the ground-state charge density redistribution, $\Delta\rho(\mathbf{r}) = \rho_{\text{cluster}}(\mathbf{r}) - \sum_i \rho_{\text{atoms}}(\mathbf{r} - \mathbf{r}_i)$, for all three dimers.

In the pristine Co_2 case, we get a Δ_g ground-state with $\mu = 4\mu_B$, a short bond length $d_{\text{Co–Co}} = 1.97$ Å and a large binding energy, $E_b = 1.50$ eV. Although these results are consistent with previous DFT reports, collision-induced dissociation (CID) experiments (Hales et al. 1994) have estimated an upper bound of $E_d = 1.32$ eV for the Co_2 dimer. The nature of the Co_2 bond is related to a contribution of an antibonding d-σ_u^* molecular orbital (Jamorski et al. 1997). As a benchmark test, we also calculated this case using other GGA potentials, and the result for PW91 is $E_b = 1.73$ eV, while LSD (no GGA) gives a higher $E_b = 2.32$ eV. Bond lengths and magnetic moments do not change appreciably.

In the opposite pristine Cu_2 case, a larger bond length $d_{\text{Cu–Cu}} = 2.22$ Å and a smaller $E_b = 1.13$ eV are obtained. The ground-state electronic structure is $(3d^{10})\,(3d^{10})\,(4s\sigma_g^2)$. The experimentally accepted CID value is $E_d = 1.04$ eV (Rohlfing and Valentini 1986).

Table 1 Summary of the ground-state properties of Co–Cu clusters, from dimers to hexamers, including: point symmetry groups; binding energies per atom E_b (in eV); experimental dissociation energies per atom E_d (in eV); total magnetic moments μ (in μ_B: bohr magnetons); average bond lengths $d_{Co–Co}$, $d_{Co–Cu}$ and $d_{Cu–Cu}$ (in Å) between closest atomic species; ionization potentials IP (in eV); and electron affinities EA (in eV)

Cluster	Symmetry	E_b (eV)	E_d (eV)[a]	μ (μ_B)[b]	$d_{Co–Co}$ (Å)	$d_{Co–Cu}$ (Å)	$d_{Cu–Cu}$ (Å)	IP (eV)	EA (eV)
Co_2	Δ_g	1.50	1.32	4 (4)	1.97	–	–	5.40	2.33
CoCu	Δ_u	1.05	–	2 (2)	–	2.24	–	5.66	2.17
Cu_2	Δ_g	1.13	1.04	0 (0)	–	–	2.22	6.56	2.36
Co_3	C_{2v}	1.86	1.45	7 (7)	2.20	–	–	4.67	2.63
Co_2Cu	–	1.63	–	5 (5)	2.03	2.26	–	5.73	2.60
$CoCu_2$	C_{2v}	1.31	–	1 (3)[c]	–	2.39	2.29	4.47	2.73
Cu_3	D_{3h}	1.22	0.96	1 (1)	–	–	2.33	4.73	2.71
Co_4	D_{2d}	2.33	2.41	10 (10)	2.23	–	–	5.42	2.30
Co_3Cu	C_{2v}	2.07	–	6 (6)	2.18	2.39	–	4.89	2.75
Co_2Cu_2	–	1.84	–	4 (4)	2.05	2.37	2.36	5.06	2.78
$CoCu_3$	C_{2v}	1.60	–	2 (2)	–	2.36	2.35	5.22	2.70
Cu_4	D_{2h}	1.58	2.38	0 (0)	–	–	2.35	5.48	2.74
Co_5	D_{3h}	2.61	2.84	13 (13)	2.34	–	–	5.08	2.67
Co_4Cu	–	2.37	–	9 (11)[c]	2.33	2.39	–	4.85	2.88
Co_3Cu_2	C_{2v}	2.13	–	7 (7)	2.21	2.35	3.36	5.04	2.62
Co_2Cu_3	–	1.96	–	5 (5)	2.07	2.39	2.39	5.08	2.80
$CoCu_4$	C_{2v}	1.81	–	3 (3)	–	2.31	2.37	5.00	3.01
Cu_5	C_{2v}	1.71	1.72	1 (1)	–	–	2.36	5.56	2.88
Co_6	O_h	2.98	3.31	14 (14)	2.27	–	–	5.07	1.67
Co_5Cu	O	2.71	–	12 (12)	2.27	2.41	–	4.90	2.82
Co_4Cu_2	–	2.51	–	10 (10)	2.27	2.41	2.44	4.92	2.82
Co_3Cu_3	–	2.31	–	8 (8)	2.24	2.39	2.46	5.13	2.96
Co_2Cu_4	–	2.10	–	6 (6)	2.15	2.41	2.43	5.25	3.16
$CoCu_5$	C_5	1.98	–	2 (2)	–	2.33	2.44	5.03	2.54
Cu_6	D_{3h}	1.90	2.18	0 (0)	–	–	2.36	6.16	2.20

[a] Values of E_d for Co_n: from Hales et al. (1994), for Cu_n: from Rohlfing and Valentini (1986), and Jaque and Toro-Labbé (2004)

[b] From this study and (between parentheses) from the ultimate jellium model: Koskinen et al. (1995), Kolehmainen et al. (1997)

[c] Only these two magnetic cases differ from the ultimate jellium model. See "Magnetic moment" section for a thorough discussion

This situation is foremost linked to localized 3*d* and delocalized 4*s* electrons, both contributing strongly to the chemical bonding (Leopold and Lineberger 1986; Jaque and Toro-Labbé, 2002, 2004; Datta et al. 2007).

In the diatomic CoCu case, the binding energy ($E_b = 1.05$ eV) is found even smaller than in Cu_2, resulting in the largest dimer bond length ($d_{Co–Cu} = 2.24$ Å). This can be understood if we look at the density redistribution around the atoms. From Fig. 1 we see a multipole pattern with antinodal lines directed outside the Co atoms (coming from the antibonding nature of the bond), whereas no such large density redistribution is seen around Cu atoms (because of their filled *d*-orbital shells). This reflects a stronger electrostatic repulsion of the Co *d*-electrons, which might be responsible for the reduction of the CoCu binding energy, as compared to the pristine dimers.

As for relativistic effects, we have done a second PBE benchmark calculation for the pristine dimers, including spin-orbit corrections (SOC), and the results for the ground-state are a new $E_b = 1.51$ eV for Co_2, while a new $E_b = 1.12$ eV for Cu_2. Namely, less than 1 per cent of change from our results given in Table 1. As larger clusters are made of these basic units, we conclude from this quantitative test that relativistic

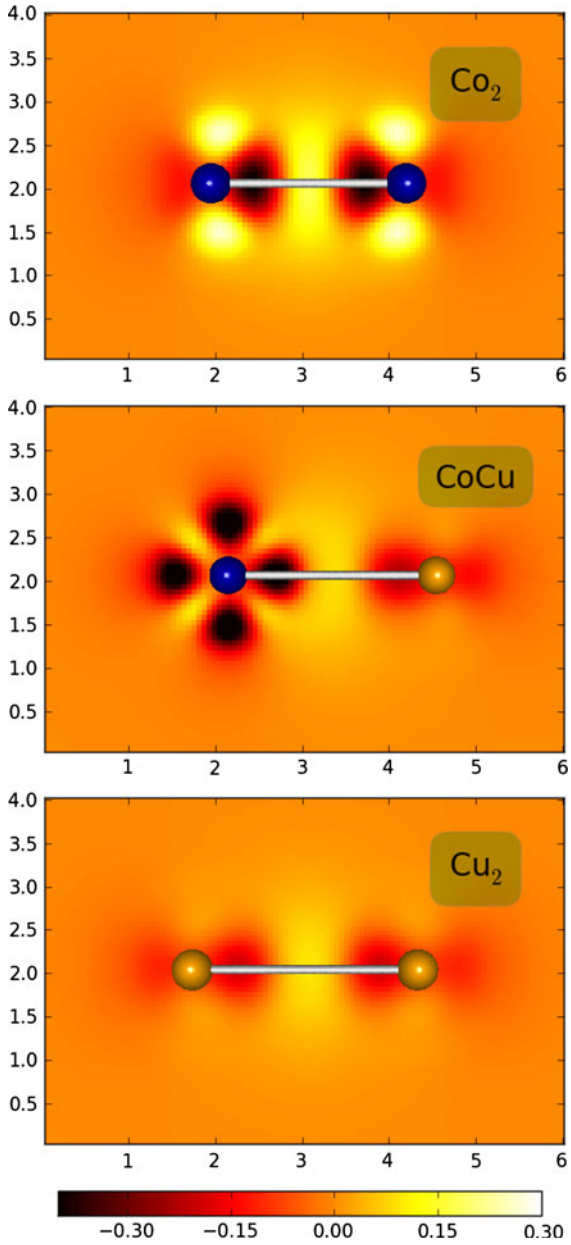

Fig. 1 Dimers: isodensity contour plots of $\Delta\rho$, the difference of the electron charge density between the cluster and the individual atoms in the ground-state for Co_2, CoCu, and Cu_2 dimers, from *top* to *bottom*. Atomic distances are in Å and the *colorbar* is in e/Å^3 units. The larger variation of charge density around the Co atoms, but not much on Cu atoms, reflects the partial occupancy of the directional *d* orbitals of cobalt. This makes the surroundings of Co atoms more flexible for chemical bonding, a common fact for all Co–Cu clusters. (Color figure online)

effects are unimportant for small Co–Cu clusters, as it is also qualitatively expected for these light transition metals.

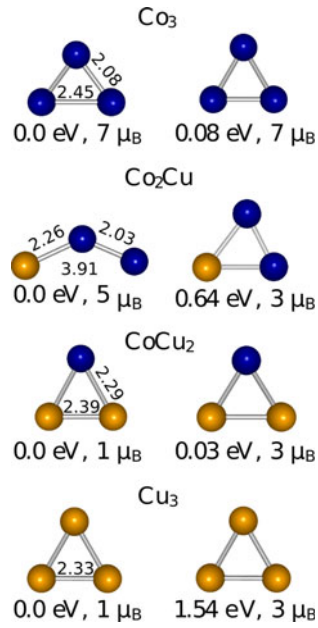

Fig. 2 Trimers: geometric structures for the ground-state (*left-column*) and its first isomers (*right-column*) for $Co_{3-m}Cu_m$ clusters, for $m = 0, 1, 2, 3$, from *top* to *bottom*. Co and Cu atoms are, from now on, marked as *blue* and *yellow* balls, respectively. Only the relevant bond lengths (in Å) for the ground-states are indicated. The relative energies with respect to the ground-state (ΔE, in eV) and the cluster magnetic moments (in μ_B) are given below every single configuration

We further acknowledge another (non PBE) numerical approach for the nonmagnetic Cu_2, based on relativistic XC potentials and developed at the LDA level (Kullie et al. 2008) which obtains $E_b = 1.39$ eV. Thus, even a fully relativistic (Dirac) LDA method does not stay closer to the available experimental data. Henceforth, new developments are expected for further accurate GGA relativistic corrections with basis-dependent XC density functionals, along the lines of Wang and Liu (2005), for example.

Trimers

The two Co_3 clusters (see Fig. 2) have Jahn–Teller isosceles (C_{2v}) triangular structures in the ground-state and in the first isomer state, as in some previous reports (Castro et al. 1997; Jamorski et al. 1997; Datta et al. 2007). The ground-state structure is an obtuse triangle, with a longer bond length at the base (2.45 Å) and two shorter equal sides (2.08 Å), while the first isomer configuration is an acute triangle, with the two longer equal sides (2.22 Å) and a short basal bond

length (2.08 Å). Notice that bond lengths given in Table 1 are, in contrast, average ground-state values. The equilateral (D_{3h}) Co_3 trimer (not shown) lies $\Delta E = 0.63$ eV above the ground-state energy and is not stable (saddle-point).

For the Co_2Cu ground-state we found a scalene triangle with a shrinked (2.03 Å) Co–Co bond length. For completeness, and because of the quasi-linearity of this case, we have also calculated explicitly the two possible linear arrangements (not shown): the Cu–Co–Co, which lies $\Delta E = 1.0$ eV above, and the Co–Cu–Co, which lies $\Delta E = 1.74$ eV above the corresponding ground-state depicted on Fig. 2.

The two $CoCu_2$ clusters, on the other hand, are obtuse (C_{2v}) triangles and they lie very close in energy. They differ mainly in the magnetic moment and in the basal Cu–Cu bond (0.1 Å longer in the isomer state). We see from Table 1, that in this particular case we have a different magnetic moment in the ground-state from that of the ultimate jellium model. We come back to this fact in Magnetic moment section.

In the Cu_3 cluster, the ground-state and the first isomer are both magnetic, both have equilateral (D_{3h}) triangles, similar to previous reports (Kabir et al. 2004a, b), although they have different bond lengths and different magnetic moments (see Fig. 2). The first isomer is also unexpectedly far in energy, $\Delta E = 1.54$ eV above the ground-state.

Tetramers

The Co_4 cluster (see Fig. 3) has a magnetic ground-state configuration which is a 3D distorted (D_{2d}) tetrahedron with one pair of long bonds (2.71 Å) and two pairs of short bonds (2.14 Å), as in previous reports (Castro et al. 1997; Jamorski et al. 1997; Datta et al. 2007; Ganguly et al. 2008). This 3D distorted configuration is related to the Jahn–Teller effect, since it has a reduced energy as compared to the symmetric third isomer (T_d) tetrahedron case, which lies $\Delta E = 0.65$ eV above in energy. In contrast, the first isomer has a planar rhombus configuration (D_{2h}) with a $\Delta E = 0.06$ eV, while the second isomer is a planar square configuration (D_{4h}) with $\Delta E = 0.18$ eV above the ground-state energy.

We notice from Fig. 3 that unlike Co_4, all ground-states have similar 2D geometries, namely, distorted rhomboidal structures ending with a symmetric (D_{2h}) rhombus for Cu_4. Concomitantly, there is a jump of $4\mu_B$ from Co_4 to Co_3Cu. We also see that the first isomers of Co_3Cu, Co_2Cu_2, $CoCu_3$ and Cu_4 are rather far above the ground-state energy. Therefore, except for Co_4, they are very unlikely to be mixed in any experimental situation at room temperature.

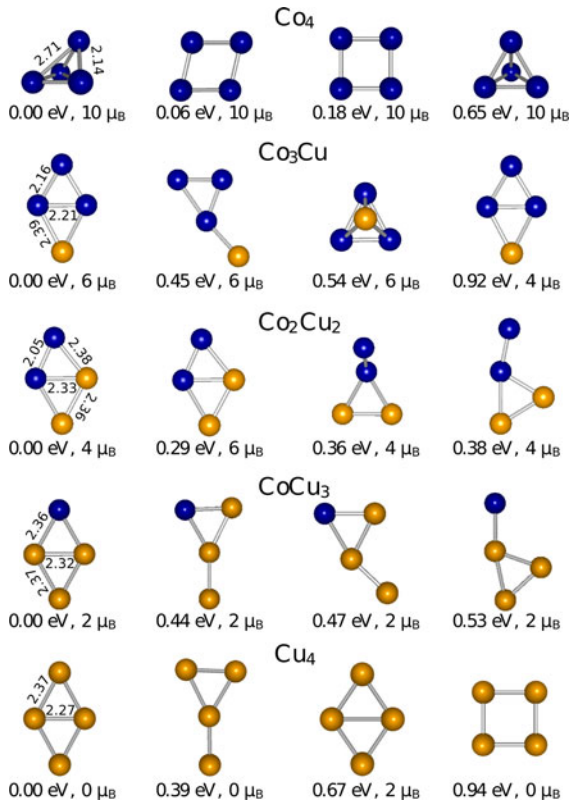

Fig. 3 Tetramers: ground-state structures and the first three low-energy isomers for $Co_{4-m}Cu_m$ clusters, for $m = 0, 1, 2, 3, 4$, from *top* to *bottom*. We use the same conventions as in Fig. 2. Only the relevant bond lengths (in Å) for the ground-states (*left-column*) are indicated. Clumping of Co atoms is observed, here and in the next examples

For every single configuration, one can also see a global tendency of Co atoms to agglomeration, with the Co atoms forming close-packed clumps. This behavior can be traced back to the stronger Co–Co interaction found in dimers and trimers and it extends to larger clusters as well. Such a trend would lead to segregation in bulk Co–Cu alloys (Rabedeau et al. 1993; Miranda et al. 2003, 2006; Fan et al. 2004).

One can also see from Fig. 3 that the minima d_{Co-Cu} and d_{Cu-Cu} bond lengths for tetramers are almost constant for all Cu concentrations. In contrast, the minima d_{Co-Co} change appreciably indicating a stronger chemical bonding.

Pentamers

In $Co_{5-m}Cu_m$ clusters (Fig. 4) we see either cumpling of Co atoms and also some homotopes, i.e., configurations with the same geometric structures but of different atomic species placed at different sites. Another phenomenon that occurs is a 2D to 3D shape transition for the ground-states as the number of Co atoms increase. For instance, the Cu_5 ground-state structure is a planar (C_{2v}) trapezoid and the series of $CoCu_4$, Co_2Cu_3, Co_3Cu_2 and Co_4Cu adopt flake-like ground-state structures gradually increasing its curvature, ending with a cage-like 3D hexahedron (D_{3h}) for the Co_5 ground-state.

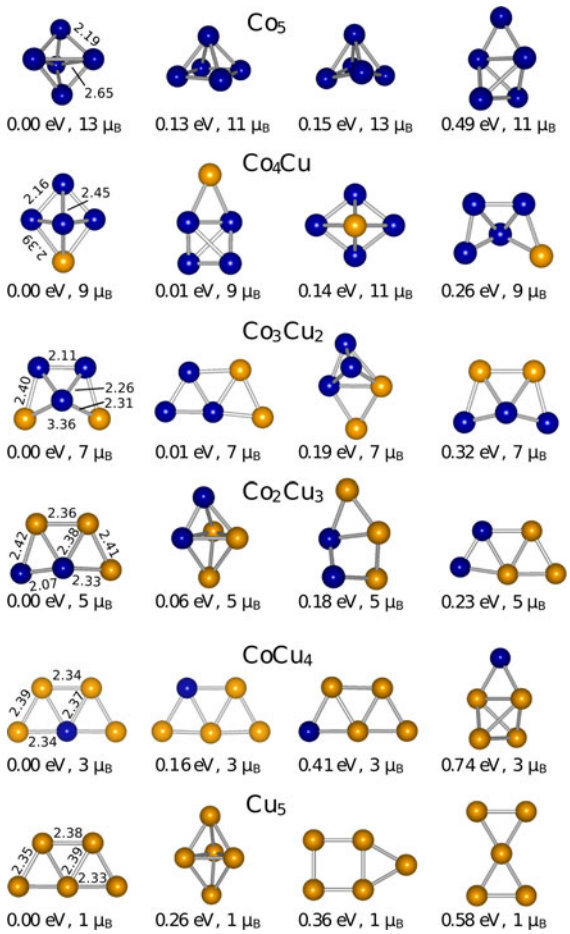

Fig. 4 Pentamers: ground-state structures and the first three low-energy isomers for $Co_{5-m}Cu_m$ clusters, for $m = 0, 1, 2, 3, 4, 5$, from *top* to *bottom*. Same conventions as in Fig. 2. Besides cumpling of Co atoms and the presence of homotopes, we also observe a 2D to 3D geometrical transition in the ground-state configurations (*left-column*), placed around Co_4Cu, when going from Cu_5 to Co_5

This Co_5 ground-state hexahedron can also be described as a trigonal bipyramid (TBP), composed by six triangles with the atoms located at the vertices. These obtuse triangles have two equal short sides of 2.19 Å sharing the apex Co atoms and basal long sides of 2.65 Å. The first isomer is a square (C_{4v}) pyramid $\Delta E = 0.13$ eV above in energy.

The Co_4Cu ground-state structure is a distorted TBP (or rhombus pyramid), with two $d_{Co–Co}$ bond lengths of 2.16 Å and three of 2.45 Å length. There are also three $d_{Co–Cu}$ bond lengths of 2.39 Å. We notice that the first isomer is very close in energy, $\Delta E = 0.01$ eV above the ground-state. This is the second case we found to differ in the magnetic moment from the ultimate jellium model, as quoted in Table 1. We shall discuss this case in more detail on "Magnetic moment" section .

Another example of flake (2D) structure is the Co_3Cu_2 ground-state, which is composed by an acute isosceles Co trimer, with two equal bonds of 2.26 Å and one base bond of 2.11 Å, plus two extra Cu atoms sticked to the sides by 2.40 and 2.31 Å $d_{Co–Cu}$ bond lengths, respectively, thus forming a deformed trapezoid with a very large $d_{Cu–Cu}$ bond distance of 3.36 Å, as indicated in Fig. 4.

The flake geometry is still observed in Co_2Cu_3 ground-state, but is more planar and also distorted. The distortion is attributed to the $d_{Co–Co}$ bond length, which is shrinked to 2.07 Å, quite short if compared to the other bonds in the pentamer clusters.

An increase of symmetry is obtained in the $CoCu_4$ case, where the ground-state has an almost planar (C_{2v}) trapezoid. This 2D configuration has indeed various homotopes among the different configurations in Fig. 4.

Finally, the pristine Cu_5 ground-state structure is completely planar (C_{2v}), and as mentioned above this happens in the absence of Co atoms. It is not a regular trapezoid because such structure may be thought of as composed by an equilateral Cu trimer with 2 lateral side linked Cu atoms.

Contrary to the tetramers, the series of Co_4Cu, Co_3Cu_2 and Co_2Cu_3 first isomers all have a very small energy difference ΔE to their ground-states. That is not the case for the pristine cases, Co_5 and Cu_5. Besides, the higher E_b in $CoCu_4$ than in Cu_5 ground-states (see E_b values in Table 1) confirms the stronger Co–Cu over Cu–Cu bonding.

Hexamers

The geometry of the Co_6 ground-state is a 3D regular (O_h) octahedron, whose sides are all equal to 2.27 Å, as seen from Fig. 5. A slightly distorted (D_{4h}) octahedron appears as the first isomer, separated $\Delta E = 0.88$ eV above in energy.

Similarly, the ground-state structure of Co_5Cu also has an octahedral configuration, which is not regular due to its apex Cu atom. This Cu atom produces an elongation of the $d_{Co–Cu}$ bond lengths to 2.41 Å, an elongation of the apical $d_{Co–Co}$ bond lengths to 2.30 Å, and a shrinking of the equatorial $d_{Co–Co}$ bond lengths to 2.24 Å.

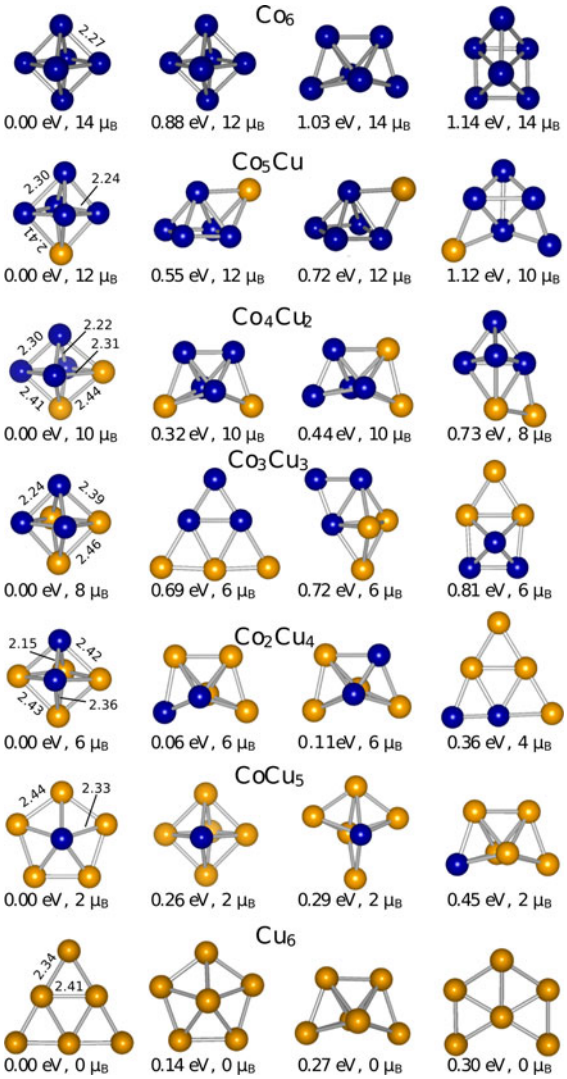

Fig. 5 Hexamers: ground-state structures and the first three low-energy isomers for $Co_{6-m}Cu_m$ clusters, for $m = 0, 1, 2, 3, 4, 5, 6$, from *top to bottom*. Same conventions as in Fig. 2. An earlier 2D to 3D transition in the ground-state configurations (*left-column*) occurs here, when going from Cu_6 to Co_6. We place it arbitrarily at $CoCu_5$

The ground-state configuration of the Co_4Cu_2 ground-state, the substitution of another Co by a Cu atom occurs by clumping it to the previous Cu atom (and not by biapical occupancy, for instance), thus confirming our rule of close-packed Co clumps of the previous subsections. This substitution produces a distorted octahedron, as seen from Fig. 5.

The ground-state configuration of the Co_3Cu_3 cluster is another distorted octahedron, which can be seen as composed by two equilateral trimers. One is a Co trimer with bond lengths of 2.24 Å and the other is a Cu trimer with bond lengths of 2.46 Å. They are linked by $d_{Co–Cu}$ bonds lengths equal to 2.39 Å.

The last distorted octahedral ground-state configuration in this series is the Co_2Cu_4 case. We have here, two neighboring Co atoms with a small 2.15 Å $d_{Co–Co}$ bond length, two relaxed 2.42 Å and one 2.36 Å $d_{Co–Cu}$ bond lengths, and five large $d_{Cu–Cu}$ bond lengths of 2.43 Å.

On the other hand, the $CoCu_5$ ground-state structure has an interesting geometry, as seen from Fig. 5, which we have reproduced in more detail in Fig. 6 using a density contour plot. The geometry is a (C_5) pyramid with a pentagonal basis of Cu atoms, and with the Co atom at the apex position, thus forming an almost planar flake structure. The Cu atoms are linked by 2.44 Å bond lengths, while the Co–Cu bond lengths are 2.33 Å. The main feature of this cluster is the pentagonal arrangement of the Cu atoms coating the central Co atom. Due to such symmetric charge redistribution, this cluster is very unlikely to donate or accept an electron as compared to the other hexamers, making this configuration very stable and symmetric. Notice also the jump of $4\mu_B$ in going from $CoCu_5$ to Co_2Cu_4 ground-states.

Finally, the ground-state of Cu_6 is a planar (D_{3h}) structure, which is composed (see Fig. 5) by an inner equilateral Cu trimer made of equal 2.41 Å bond lengths, together with 3 outer Cu atoms linked by 2.34 Å bond lengths, respectively.

Binding energy and stability

In this and the following sections we focus our attention on the global behavior of the clusters with

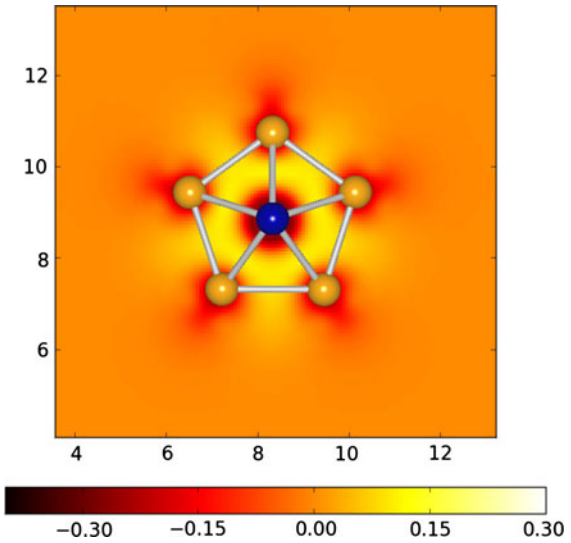

Fig. 6 Isodensity contour plot of $\Delta\rho$, the electron charge density difference between the cluster and the individual (separated) atoms in the $CoCu_5$ ground-state pyramidal configuration. Same conventions as in Fig. 1. Although it has a dihedral angle of 27.6°, we shall consider it as planar (i.e., 2D geometry) for the magnetic moment results. A circular depleted zone is observed around the apex Co atom. This allocated charge redistributes forming a covalent bond along the atomic bonds. Such inter-ionic strong bonding is mostly provided by the partially filled directional orbitals of the Co *d*-shell, as well as by *s*-electrons coming from elsewhere. (Color figure online)

increasing Cu concentration and for different cluster sizes, at the ground-state level, using the physical descriptors defined above.

In Fig. 7 we present the binding energy E_b per atom. A general monotonic decrease with the Cu concentration and a monotonic increase as a function of cluster size is observed. This outcome is due to the stronger binding among Co atoms as compared to the weak binding among Cu atoms and also a weak Co–Cu binding, as shown in the previous sections. Therefore, a larger concentration of Co atoms makes these bimetallic clusters energetically more favorable. The only exception to this rule is the Co_1Cu_1 dimer, which has an E_b slightly lower than the Cu_2 dimer. As was explained in relation to Figs. 1 and 6, this is basically due to the partially-filled Co core cloud, which is more cohesive than the (less flexible) completely filled Cu *d*-shell.

In Fig. 8 we show a comparison of the minima $d_{Co–Co}$, $d_{Co–Cu}$, and $d_{Cu–Cu}$ bond lengths, averaged over the ground-states shown in the previous section. We can see that, in the mean, the Co–Cu and Cu–Cu

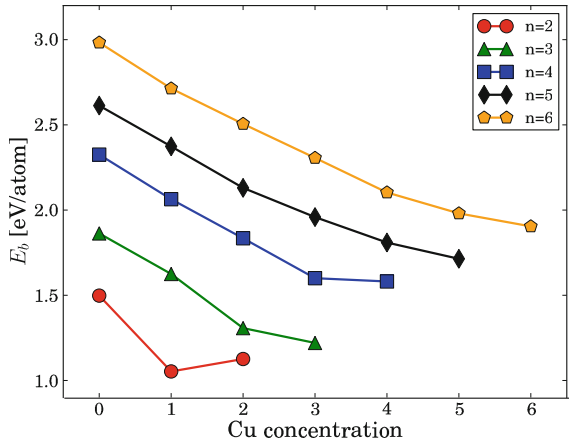

Fig. 7 Binding energies E_b per atom of the $Co_{n-m}Cu_m$ clusters versus *m*, the Cu content. Clusters of equal sizes (*n*) are joined with *lines* to guide the eye. A global monotonic decrease of E_b with Cu content is seen (with one exception at Co_1Cu_1). We also observe a global increase of E_b per atom with the clusters size

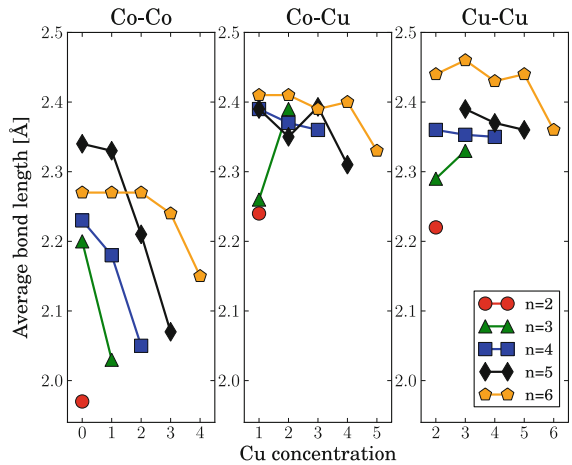

Fig. 8 Average bond lengths Co–Co, Co–Cu, and Cu–Cu of nearest atoms of the $Co_{n-m}Cu_m$ clusters as a function of the Cu concentration *m*, for different cluster sizes *n*. The Co–Co bond lengths are, on *the average*, *the smallest ones*, indicating a large cohesive behavior

bond lengths are quite similar and larger than the Co–Co bond lengths. The latter increase with Co concentration, except for $n = 6$ clusters, where they saturate at $m = 2$ (Co_4Cu_2 case). This finite-size effect of the Co–Co interaction strength with the cluster size is an open question, which may require larger clusters ($n > 6$) to be calculated. Due to scaling laws for the cohesive energy with the interatomic distance ($\sim d^{-6}$), we can say in view of these trends that, on average, a

large cohesive behavior driven by the Co atoms is observed in these clusters, which indicates consequently a strong tendency for segregation in the bulk.

The relative stability (S) for bimetallic Co–Cu clusters of sizes $n = 4, 5, 6$, as a function of Cu concentration is shown in Fig. 9. According to our definition in Eq. (3), the smaller the value of S the larger stability we have, as compared to its m-neighbors, for a fixed cluster size n. Therefore, in the $n = 4$ case, the Co_2Cu_2 cluster is seen to have maximum stability, which is probably due to the inclusion of a Co_2 dimer as part of it. In the $n = 5$ case, the maximum stability appears for the Co_4Cu cluster, for which the inclusion of a Co_4 tetramer seems to be most stable. In addition, there is a local stability for the Co_2Cu_3 cluster, but relaxed. The maximum stability for $n = 6$ is for the Co_3Cu_3 cluster, maybe because of the inclusion of a Co_3 trimer. These stability results support another, but different, evidence for the tendency of segregation of Co in the presence of Cu atoms. In our results, this trend is observed through Co clumping whose relative stability is stoichiometrically very size-dependent.

Magnetic moment

Magnetic properties have been investigated only for pristine Co_n clusters (Fan et al. 1997; Datta et al. 2007; Dong and Gong, 2008). We found, as in previous references, that the Co–Co interactions are ferromagnetic for the entire size range studied. In Fig. 10 we show the total magnetic moment of the ground-state configurations as a function of Cu concentration for different cluster sizes. In general, we see a linear increase of $2\mu_B$ with the amount of Co atoms, with some exceptional jumps where the difference of two nearest configurations is $4\mu_B$ (and one particular case, Cu_1Co_2, with no increase). One way to understand the behavior of the magnetic moments is as follows: each Co atom present in the cluster generates an amount of $2\mu_B$ for the magnetic moment because of the well localized charge in the d-shell, i.e., by keeping almost intact its atomic $3d^8 4s^1$ configuration with two unpaired d-electrons. This trend has been further verified by integrating the charge density around the Co atoms on each cluster, within a 1.3 Wigner–Seitz radius, and checking that the number of electrons was 8 and the magnetic moment was ~$2\mu_B$ within 99 per cent. The extra magnetic moment of some structures, or $4\mu_B$ jumps as previously named, is given by unpaired s-type electrons distributed along the bonds, which we may call as *itinerant magnetism*.

The electronic behavior of these s-type electrons, on the other hand, is very similar to that of the ultimate or deformable jellium model (Koskinen et al. 1995; Kolehmainen et al. 1997). In this model, the positive background charge is allowed to deform, or adjust, to the shape of the electronic density which is in turn

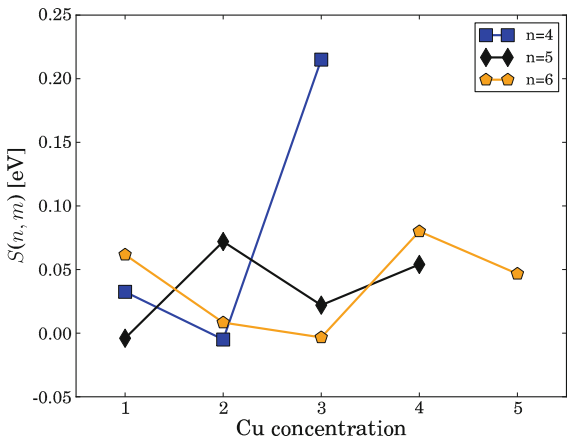

Fig. 9 Relative stability (S) of the $Co_{n-m}Cu_m$ clusters for some sizes $n = 4, 5, 6$ as a function of the Cu concentration m (for $1 \leq m \leq 5$). According to Eq. (3), small values of S indicate a large stability

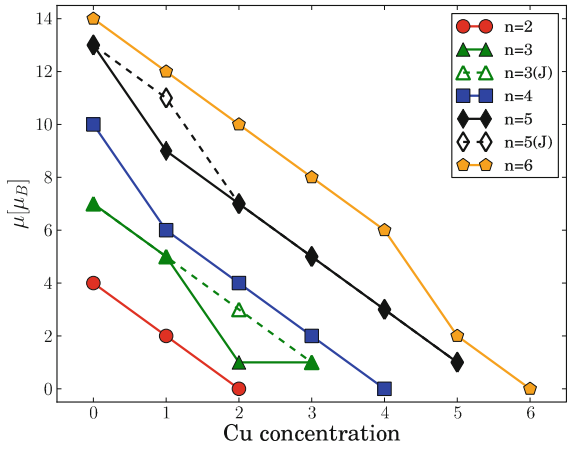

Fig. 10 Total magnetic moment μ of $Co_{n-m}Cu_m$ clusters, where m is the Cu concentration and n is the cluster size. Our results (*full symbols*) are shown to differ in two anomalous cases from those of the ultimate jellium (J) model: $CoCu_2$ and Co_4Cu (*open symbols*)

calculated within DFT theory. Although a somewhat simplified version of the DFT algorithm employed here, this model can explain the magnetic behavior of these Co–Cu clusters in most of the structures analyzed in this study. Their non-trivial DFT results can be summarized as follows: If we have N_s valence electrons then they are ordered in different energy levels, depending on whether they are distributed in 2D or 3D configurations, by applying the Pauli principle and Hund rules for interacting electrons. The magnetic moments are therefore as given in Table 2.

The 2D results of the ultimate jellium model (first row of Table 2) can be seen from the rightmost end of the lines drawn in Fig. 10: even and odd pristine Cu_n clusters end up with 0 or $1\mu_B$, respectively. The ground-state configurations of these Cu_n clusters were demonstrated to be planar (2D) in "Geometric structures" section . Moreover, every observed jump of $4\mu_B$ in Fig. 10 can be understood as a transition from the 2D to the 3D row in Table 2, as it is easily verified by inspecting the geometric results depicted in "Geometric structures" section: every time that a 2D to 3D transition occurs in the ground-state configuration we have the $4\mu_B$ jump. For example, in the $CoCu_5$ case (use $N_s = 6$) we have: $2\mu_B$ (1Co) + $0\mu_B$ (2D) = $2\mu_B$, while in the Co_2Cu_4 case: $4\mu_B$ (2Co) + $2\mu_B$ (3D) = $6\mu_B$. Hence, the ultimate jellium model accounts for most of our results, except in the $CoCu_2$ and Co_4Cu cases. These two particular cases cannot be explained by this model because we have a considerable contribution of unpaired *s*-electrons along the bonds, as was numerically verified through the projection onto *s*- and *d*- orbitals in these cases: a large contribution of interatomic charge density was seen, as in the examples illustrated in Figs. 1 and 6. Obviously, the jellium model cannot afford for such inter-ionic contribution.

Table 2 Results for the magnetic moments (in μ_B) in the deformable or ultimate jellium model, where N_s is the number of valence electrons, for 2D and 3D geometrical arrangements. Adapted from Koskinen et al. (1995) and Kolehmainen et al. (1997)

N_s	2	3	4	5	6
2D	0	1	0	1	0
3D	0	1	2	3	2

Chemical properties

Chemical properties are calculated over charged systems, i.e., over cationic and anionic clusters from Eqs. (4) and (5), by changing the number of electrons $N \rightarrow N \pm 1$. In Fig. 11 we show the chemical potential μ_{chem} of the ground-state structures as a function of the Cu concentration *m*. For fixed cluster size, it has roughly a monotonic decreasing behavior with *m* (except in two cases). Namely, replacing a Co by a Cu atom *grosso modo* makes the clusters chemically more stable in the majority of cases; this might be related to the closed *d*-shell configuration of the Cu atoms.

Two ground-state structures do not follow this trend: the anomalous $CoCu_2$ and the symmetric $CoCu_5$ one (see Fig. 11). This is mostly related to big structural changes with *N*. For the $n = 6$ case, the symmetric $CoCu_5$ structure, which is approximately planar (see Fig. 6) develops a 2D to 3D geometrical transition for $N \pm 1$, and because of that the cost of putting or taking out one electron from this cluster is higher than in other structures. For the $n = 3$ case, on the other hand, the abrupt change between Co_2Cu and $CoCu_2$, as seen from Fig. 11, is also due to large changes in geometry with *N*. For instance, the $CoCu_2$ cluster undergoes approximately from an obtuse isosceles triangle (see Fig. 2) to an acute triangle of 2.29 Å basal bond length and 2.39 Å equals side bond lengths if an electron is put, and to an acute triangle

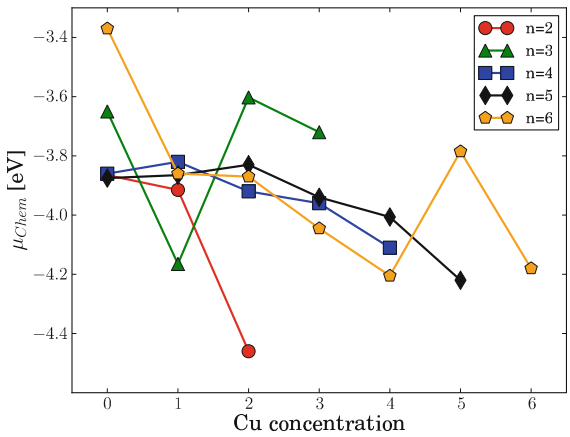

Fig. 11 Chemical potential μ_{chem} for $Co_{n-m}Cu_m$ clusters as a function of the Cu concentration. For each *n*, a rather slow decreasing behavior with *m* is seen, except in two special cases: $CoCu_2$ and $CoCu_5$

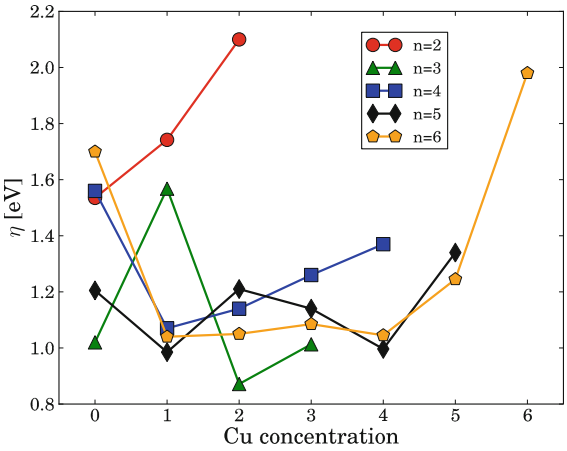

Fig. 12 Molecular hardness η for $Co_{n-m}Cu_m$ clusters as a function of the Cu concentration m. Although it seems rather size-dependent, some general trends can be extracted from this behavior. One of them is the oscillatory behavior with an even/odd size n for Cu_n clusters (*rightmost end of curves*) observed experimentally. It establishes the fact that copper clusters with an even number of atoms are more stable, or less chemically reactive

with 2.02 Å basal bond length and 2.35 Å equal side bond lengths when an electron is taken out.

Finally, in Fig. 12 we show the molecular hardness η for different cluster sizes as a function of Cu content. Although it seems rather non-specific or very size-dependent for these clusters, we may describe some general trends in order to use the maximum hardness principle. First of all, except for an initial growth for the two smaller cases, $n = 2$ and 3, there is a decrease with Cu concentration for higher clusters, with an increase at the end of each series. Second, since the molecular hardness is directly related to the HOMO-LUMO gap, this means that for small η there is a greater ease to have electron excitations in those cases. Third, we observe the well-known experimental oscillating behavior with local maxima seen for pristine Cu_n clusters with even/odd n (Jaque and Toro-Labbé, 2002, 2004). This staggering effect is related to closed/open-shells (for even/odd clusters) of the Cu_n molecular orbitals, and it says that clusters with an even number of atoms are more stable (or less reactive). Fourth, if the ionization potential (IP), as given in Table 1, is plotted as a function of Cu content, we find a similar behavior to the η results, which means that $\eta \propto$ IP, except for scale, which is another way of saying that EA $\approx$ constant, or that $-\eta \propto \mu_{\text{chem}}$, throughout the series. These facts may be of interest for those trying to synthesize these novel materials.

Conclusion

In this study we proposed a full set for the most stable structural configurations of Co–Cu nanoclusters with two to six atoms based on first-principles DFT calculations. They were accurately characterized by their structural geometry, electronic binding energies, bond lengths, magnetic moments, relative stability and chemical properties. The ground-states and some low-energy isomers were given for all possible stoichiometries. We argue that the nonrelativistic PBE approach gives basically the best answers. In all cases we observe a strong tendency to agglomeration of the Co atoms. This points out to segregation processes observed in bulk Co–Cu samples. The presence of Co atoms in the clusters contribute mostly to the chemical binding but also to the formation of the magnetic moment through their partially filled core *d*-shells, giving rise to tridimensional structures. Another source for magnetism comes from unpaired valence *s*-electrons, distributed along the bonds, which partly conform the clusters binding and led to an *itinerant magnetism*. The comparison with the deformable or ultimate jellium model gives a fair agreement, if we consider a geometric 2D to 3D transition, but it fails to explain our results in some cases, particularly when the interatomic bond plays a role. We expect this trend to become more and more important for higher cluster sizes. The geometric 2D to 3D transition with the number of Co atoms is best understood if one looks at the partial electron density distribution. The Co electronic cloud, with its partially filled *d*-shell, is less rigid than that of Cu, allowing for the optimization of the binding of Co to the other atoms. This can be argued to reduce the bond lengths, to maximize the Coulomb interaction, and to increase the dimensionality of the clusters. We have also seen that the stability parameter gives another way of describing the Co clumping trend. The chemical properties, although seemed rather non-specific for six atoms, they have a regular behavior. Substituting a Co by a Cu atom, for example, makes the system chemically more stable, and the molecular hardness provides a good description of some experimental known facts.

Acknowledgements Support for this study from CNPq (Brasil) and CONICYT (Chile), Joint Project CIAM 490891/2008-0 is gratefully acknowledged. We also thank the Millennium Science Nucleus (Chile), Project P10-061-F; Doctorate Program PUC (Chile), Project 06/2009; FONDECYT (Chile), Project 1100365; and CAPES/PROCAD (Brasil) Project 059/2007. Computer time from the National Supercomputing Center CENAPAD CESUP/UFRGS is also acknowledged.

References

Bagno P, Jepsen O, Gunnarsson O (1989) Ground-state properties of third-row elements with nonlocal density functionals. Phys Rev B 40:1997–2000

Baibich MN, Broto JM, Fert A, Nguyenvan Dau F, Petroff F, Etienne P, Creuzet G, Friederich A, Chazelas J (1988) Giant magnetoresistance of (001)Fe/(001)Cr magnetic superlattices. Phys Rev Lett 61:2472–2475

Bakonyi I, Simon E, Tóth BG, Péter L, Kiss LF (2009) Giant magnetoresistance in electrodeposited Co–Cu/Cu multilayers: origin of the absence of oscillatory behavior. Phys Rev B 79:174421

Becke AD (1988) Density-functional exchange-energy approximation with correct asymptotic behavior. Phys Rev A 38:3098–310

Berkowitz AE, Mitchell JR, Carey MJ, Young AP, Zhang S, Spada FE, Parker FT, Hutten A, Thomas G (1992) Giant magnetoresistance in heterogeneous Cu–Co alloys. Phys Rev Lett 68:3745–3748

Castro M, Jamorski C, Salahub DR (1997) Structure, bonding, and magnetism of small Fe_n, Co_n, and Ni_n clusters, $n \leq 5$. Chem Phys Lett 271:133–142

Cezar JC, Tolentino HC, Knobel M (2003) Structural, magnetic, and transport properties of Co nanoparticles within a Cu matrix. Phys Rev B 68:054404

Chattaraj PK, Liu GH, Parr RG (1995) The maximum hardness principle in the Gyftopoulos–Hatsopoulos three-level model for an atomic or molecular species and its positive and negative ions. Chem Phys Lett 237:171–176

Datta S, Kabir M, Ganguly S, Sanyal B, Saha-Dasgupta T, Mookerjee A (2007) Structure, bonding, and magnetism of cobalt clusters from first-principles calculations. Phys Rev B 76:014429

Dong CD, Gong XG (2008) Magnetism enhanced layer-like structure of small cobalt clusters. Phys Rev B 78:020409

Fan HJ, Liu CW, Liao MS (1997) Geometry, electronic structure and magnetism of small Co_n ($n = 2$–8) clusters. Chem Phys Lett 273:353–359

Fan X, Mashimo T, Huang X, Kagayama T, Chiba A, Koyama K, Motokawa M (2004) Magnetic properties of Co–Cu metastable solid solution alloys. Phys Rev B 69:094432

Ferrando R, Jellinek J, Johnston RL (2008) Nanoalloys: from theory to applications of alloy clusters and nanoparticles. Chem Rev 108:845–910

Ganguly S, Kabir M, Datta S, Sanyal B, Mookerjee A (2008) Magnetism in small bimetallic Mn–Co clusters. Phys Rev B 78:014402

Ghanty TK, Banerjee A, Chakrabarti A (2010) Structures and the electronic properties of $Au_{19}X$ clusters (X = Li, Na, K, Rb, Cs, Cu, and Ag). J Phys Chem C 114:20–27

Ghosh SK, Grover AK, Chowdhury P, Gupta SK, Ravikumar G, Aswal DK, Senthil Kumar M, Dusane RO (2006) High magnetoresistance and low coercivity in electrodeposited Co/Cu granular multilayers. Appl Phys Lett 89:132507

Hales DA, Su CX, Lian L, Armentrout PB (1994) Collision-induced dissociation of Co_n^+ ($n = 2$–18) with Xe: bond energies of cationic and neutral cobalt clusters, dissociation pathways, and structures. J Chem Phys 100:1049–1057

Hickey BJ, Howson MA, Musa SO, Wiser N (1995) Giant magnetoresistance for superparamagnetic particles: melt-spun granular CuCo. Phys Rev B 51:667–669

Jamorski C, Martínez A, Castro M, Salahub DR (1997) Structure and properties of cobalt clusters up to the tetramer: a density-functional study. Phys Rev B 55:10905–10921

Jaque P, Toro-Labbé A (2002) Characterization of copper clusters through the use of density functional theory reactivity descriptors. J Chem Phys 117:3208–3218

Jaque P, Toro-Labbé A (2004) The formation of neutral copper clusters from experimental binding energies and reactivity descriptors. J Phys Chem B 108:2568–2574

Ju SP, Lo YC, Sun SJ, Chang JG (2005) Investigation on the structural variation of CoCu nanoparticles during the annealing process. J Phys Chem B 109:20805–20809

Kabir M, Mookerjee A, Bhattacharya AK (2004a) Copper clusters: electronic effect dominates over geometric effect. Eur Phys J D 31:477–485

Kabir M, Mookerjee A, Bhattacharya AK (2004b) Structure and stability of copper clusters: a tight-binding molecular dynamics study. Phys Rev A 69:043203

Knorr N, Schneider MA, Diekhöner L, Wahl P, Kern K (2002) Kondo effect of single Co adatoms on Cu surfaces. Phys Rev Lett 88:096804

Kohn W, Becke AD, Parr RG (1996) Density functional theory of electronic structure. J Phys Chem 100:12974–12980

Kolehmainen J, Häkkinen H, Manninen M (1997) Metal clusters on an inert surface: a simple mode. Z Phys D 40:306–309

Koskinen M, Lipas PO, Manninen M (1995) Electron-gas clusters: the ultimate jellium model. Z Phys D 35:285–297

Kresse G, Furthmüller J (1996a) Efficiency of ab-initio total energy calculations for metals and semiconductors using a plane-wave basis set. Comput Mat Sci 6:15–50

Kresse G, Furthmüller J (1996b) Efficient iterative schemes for ab-initio total-energy calculations using a plane-wave basis set. Phys Rev B 54:11169–11186

Kresse G, Hafner J (1993) Ab-initio molecular dynamics for liquid metals. Phys Rev B 47:558–561

Kresse G, Hafner J (1994) Norm-conserving and ultrasoft pseudopotentials for first-row and transition-elements. J Phys Condens Matter 6:8245–8257

Kresse G, Joubert D (1999) From ultrasoft pseudopotentials to the projector augmented-wave method. Phys Rev B 59: 1758–1775

Kübbler J (1981) Magnetic moments of ferromagnetic and antiferromagnetic bcc and fcc iron. Phys Lett A 81:81–83

Kullie O, Zhang H, Kolb D (2008) Relativistic and non-relativistic local-density functional, benchmark results and investigation on the dimers Cu_2, Ag_2, Au_2, Rg_2. Chem Phys 351:106–110

Leopold DG, Lineberger WC (1986) A study of the low-lying electronic states of Fe_2 and Co_2 by negative ion photoelectron spectroscopy. J Chem Phys 85:51–55

Lu QL, Zhu LZ, Ma L, Wang GH (2005) Magnetic properties of Co/Cu and Co/Pt bimetallic clusters. Chem Phys Lett 407:176–179

Mejía-López J, García G, Romero AH (2009) Physical and chemical characterization of $Pt_{12-n}Cu_n$ clusters via ab-initio calculations. J Chem Phys 131:044701

Miranda MGM, Estévez-Rams E, Martínez G, Baibich MN (2003) Phase separation in $Cu_{90}Co_{10}$ high-magnetoresistance materials. Phys Rev B 68:014434

Miranda MGM, da Rosa AT, Hinrichs R, Golla-Schindler U, Antunes AB, Martínez G, Estévez-Rams E, Baibich MN (2006) Spinodal decomposition and giant magnetoresistance. Phys B 384:175–178

Néel N, Kröger J, Berndt R, Wehling TO, Lichtenstein AI, Katsnelson MI (2008) Controlling the Kondo effect in $CoCu_n$ clusters atom by atom. Phys Rev Lett 101:266803

Parkin SSP, More N, Roche KP (1990) Oscillations in exchange coupling and magnetoresistance in metallic superlattice structures: Co/Ru, Co/Cr, and Fe/Cr. Phys Rev Lett 64: 2304–2307

Parr RG, Pearson RG (1983) Absolute hardness: companion parameter to absolute electronegativity. J Am Chem Soc 105:7512–7516

Parr RG, Yang M (1984) Density functional approach to the frontier-electron theory of chemical reactivity. J Am Chem Soc 106:4049–4050

Perdew JP (1986) Density-functional approximation for the correlation energy of the inhomogeneous electron gas. Phys Rev B 33:8822–8824

Perdew JP, Wang Y (1986) Accurate and simple density functional for the electronic exchange energy: generalized gradient approximation. Phys Rev B 33:8800–8802

Perdew JP, Wang Y (1992) Accurate and simple analytic representation of the electron-gas correlation energy. Phys Rev B 45:13244–13249

Perdew JP, Burke K, Ernzerhof M (1996a) Generalized gradient approximation made simple. Phys Rev Lett 77:3865–3868

Perdew JP, Burke K, Wang Y (1996b) Generalized gradient approximation for the exchange-correlation hole of a many-electron system. Phys Rev B 54:16533–16539

Quaas N, Wenderoth NM, Weismann A, Ulbrich RG, Schönhammer K (2004) Kondo resonance of single Co atoms embedded in Cu(111). Phys Rev B 69:201103

Rabedeau TA, Toney MF, Marks RF, Parkin SSP, Farrow RFC, Harp GR (1993) Giant magnetoresistance and Co-cluster structure in phase-separated Co–Cu granular alloys. Phys Rev B 48:16810–16813

Rastei MV, Heinrich B, Limot L, Ignatiev PA, Stepanyuk VS, Bruno P, Bucher JP (2007) Size-dependent surface states of strained cobalt nanoislands on Cu(111). Phys Rev Lett 99:246102

Rogan J, Ramírez M, Muñoz V, Valdivia JA, García G, Ramírez R, Kiwi M (2009) Diversity driven unbiased search of minimum energy cluster configurations. J Phys Condens Matter 21:084209

Rohlfing EA, Valentini JJ (1986) UV laser excited fluorescence spectroscopy of the jet-cooled copper dimer. J Chem Phys 84:6560–6566

Wang F, Liu W (2005) Benchmark four-component relativistic density functional calculations on Cu_2, Ag_2, and Au_2. Chem Phys 311:63–69

Wang CS, Klein BM, Krakauer H (1985) Theory of magnetic and structural ordering in iron. Phys Rev Lett 54:1852–1855

Wang JL, Wang G, Chen X, Lu W, Zhao J (2002) Structure and magnetic properties of Co–Cu bimetallic clusters. Phys Rev B 66:014419

Wang H, Khait YG, Hoffmann MR (2005) Low-lying quintet states of the cobalt dimer. Mol Phys 103:263–268

Xiao JQ, Jiang JS, Chien CL (1992) Giant magnetoresistance in nonmultilayer magnetic systems. Phys Rev Lett 68:3749–3752

Yang M, Jackson KA, Koehler C, Frauenheim T, Jellinek J (2006) Structure and shape variations in intermediate-size copper clusters. J Chem Phys 124:024308

Zimmermann CG, Yeadon M, Nordlund K, Gibson JM, Averback RS, Herr U, Samwer K (1999) Burrowing of Co nanoparticles on clean Cu and Ag surfaces. Phys Rev Lett 83:1163–1166